Development/Plasticity/Repair

p27^{KIP1} Regulates Neurogenesis in the Rostral Migratory Stream and Olfactory Bulb of the Postnatal Mouse

Xuekun Li,[1]* Xiaobing Tang,[1]* Beata Jablonska,[2] Adan Aguirre,[2] Vittorio Gallo,[2] and Marla B. Luskin[1]

[1]Department of Cell Biology, Emory University School of Medicine, Atlanta, Georgia 30322, and [2]Center for Neuroscience Research, Children's National Medical Center, Washington, DC 20010

Neuronal progenitor cells of the anterior subventricular zone (SVZa) migrate along the rostral migratory stream (RMS) to the olfactory bulb, where they exit the cell cycle and differentiate. The molecular mechanisms that regulate SVZa progenitor proliferation and cell-cycle exit are largely undefined. We investigated the role of p27^{KIP1} in regulating cell proliferation and survival in the RMS and olfactory bulb between postnatal day 1 (P1) and P14, the peak period of olfactory bulb neuron generation. A large proportion of cells in the RMS and the olfactory bulb express cytoplasmic p27^{KIP1}, but a small percentage display high nuclear p27^{KIP1} immunostaining, which exhibit a caudal^{low}–rostral^{high} gradient: lowest in the SVZa and highest in the glomerular layer of the olfactory bulb. p27^{KIP1} is also present in the nucleus and/or the cytoplasm of neuron-specific type III β-tubulin(+) cells. Cells with strong nuclear p27^{KIP1} expression are BrdU(−) and Ki67(−). The percentage of BrdU(+) cells in the SVZa, RMS, and olfactory bulb is higher in p27^{KIP1} null than wild-type (WT) mice at all ages analyzed. Consistent with these findings, p27^{KIP1} overexpression in cultured p27^{KIP1} null and WT SVZ cells reduced cell proliferation and self-renewal. Finally, in p27^{KIP1} null mice, the diameter of the horizontal limb of the RMS is larger than in WT mice, and development of the olfactory bulb granule cell layer is delayed, together with increased apoptotic cell density. Our results indicate that in the postnatal brain, p27^{KIP1} regulates the proliferation and survival of neuronal cells in the RMS and olfactory bulb.

Introduction

The production of interneurons in the olfactory bulb originates from neuronal progenitor cells derived from the anterior part of subventricular zone (SVZa) (Luskin, 1993; Lois and Alvarez-Buylla, 1994; Menezes et al., 1995). Previous studies demonstrated that in mice most of the granule and periglomerular cells in the olfactory bulb are generated between embryonic day 18 (E18) and postnatal day 5 (P5) (Hinds, 1968). SVZa-derived neuronal progenitors tangentially migrate along the rostral migratory stream (RMS) to the olfactory bulb, where they radially migrate and differentiate into interneurons of the granule cell layer (gcl) and glomerular layer (gl) (Luskin, 1993; Lois and Alvarez-Buylla, 1994). The molecular mechanisms that regulate SVZa neuronal progenitor proliferation and differentiation in the RMS and olfactory bulb are not fully determined.

Progression of the cell cycle from G_1 to S phase is positively regulated by cyclin-dependent kinases (CDKs), including CDK2 and CDK4, and negatively modulated by two families of CDK inhibitors (CDKIs), the INK4 and the CDK-inhibitory protein (CIP)/kinase-inhibitory protein (KIP) families (Sherr and Roberts, 1995). INK4 includes p16^{INK4a} (p16), p15^{INK4b} (p15), p18^{INK4c} (p18), and p19^{INK4d} (p19). The CIP/KIP family comprises p21^{CIP1} (p21), p27^{KIP1} (p27), and p57^{KIP2} (p57). p27 null [p27 knock-out (p27KO)] mice display a larger brain size (Fero et al., 1996; Kiyokawa et al., 1996). Several reports demonstrated that p27 regulates many aspects of neurogenesis, including neural progenitor proliferation, migration, and/or differentiation (Zindy et al., 1999; Levine et al., 2000; Miyazawa et al., 2000; Legrier et al., 2001; Cunningham et al., 2002; Doetsch et al., 2002; Goto et al., 2004; Nguyen et al., 2006). All these studies indicate that p27 plays critical roles in the development of the CNS (Cunningham and Roussel, 2001).

The spatial and temporal pattern of p27 expression in the RMS and olfactory bulb during the peak period of neurogenesis is still unknown. Furthermore, a functional role for p27 as a regulator of neuronal cell proliferation and survival in the RMS and olfactory bulb during this developmental process is still undefined. This information would be essential to understand specific aspects of olfactory bulb development during the first 2 postnatal weeks (i.e., during the period of maximal growth of this region in mice).

In the present study, we investigated p27 expression and regulation in cells of the mouse SVZa, RMS, and olfactory bulb during the first 2 weeks of postnatal development. We also studied p27 function in neural cell proliferation and survival in the same brain regions. We demonstrate that the spatiotemporal expression pattern of p27 is consistent with a role of this CDKI as an

Received Aug. 25, 2008; revised Dec. 19, 2008; accepted Dec. 29, 2008.

This work was supported by National Institute of Deafness and Other Communicative Disorders Grant R01 DC03190 (M.B.L.) and National Institute of Neurological Disorders and Stroke Grants R01 NS045702 (V.G.) and K99 NS057944 (A.A.). We thank Dr. Douglas Falls (Emory University) for help with analysis of the results. We also thank Drs. Martine Roussel and Frederique Zindy (Saint Jude Children's Research Hospital, Memphis, TN) for providing p27^{KIP1} null mouse founders. We thank Dr. Susan Winandy (Northwestern University Feinberg School of Medicine, Chicago, IL) for generously providing the p27^{KIP} retroviral construct.

*X.L. and X.T. contributed equally to this work.

Correspondence should be addressed to Dr. Marla B. Luskin, Department of Cell Biology, Emory University School of Medicine, Whitehead Biomedical Research Building, 615 Michael Street, Room 548, Atlanta, GA 30322. E-mail: luskin@cellbio.emory.edu.

X. Li's present address: Department of Human Genetics, Emory University School of Medicine, Atlanta, GA 30322.

DOI:10.1523/JNEUROSCI.4051-08.2009

 0270-6474/09/292902-13$15.00/0

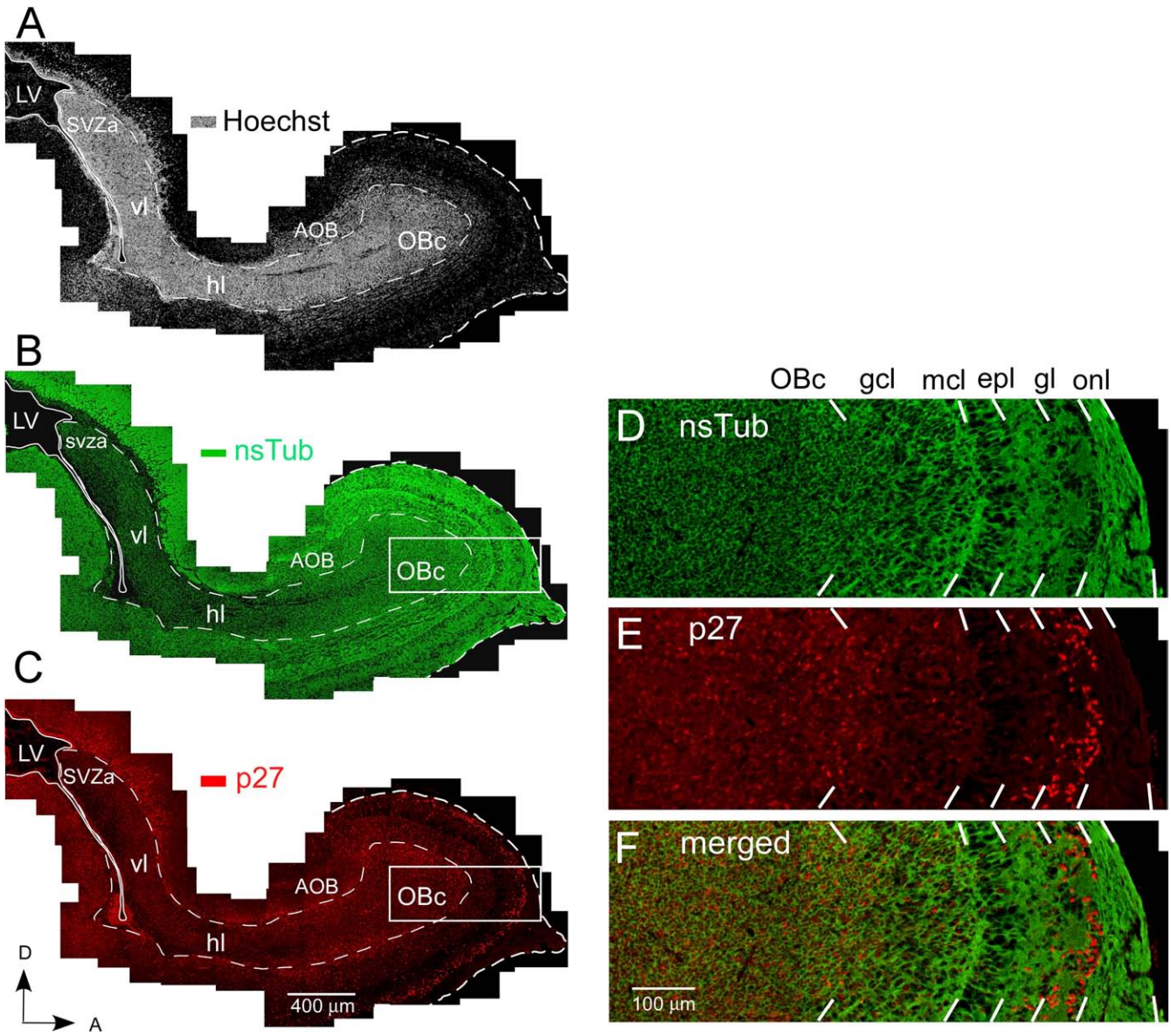

Figure 1. Overview of p27 expression in the WT mouse at P1 in the RMS and neuronal cell layers of the olfactory bulb. ***A–C***, Identical parasagittal section stained with Hoechst 33342 (***A***), anti-nsTub (***B***), and anti-p27 (***C***). ***A***, Bright-field photomicrograph of a parasagittal forebrain section stained with the nuclear dye Hoechst 33342 showing intense labeling of the RMS, which contains a high cell density compared with the surrounding brain regions. The four regions of the RMS labeled along its caudal–rostral axis are as follows: (1) the SVZa, an enlarged region of the SVZ overlying the anterior horn of the lateral ventricle; (2) the vl, a short segment of the RMS that descends ventrally from the SVZa; (3) the hl, the rostral extension of the RMS; and (4) the OBc, the terminal portion of the RMS in the center of the olfactory bulb. ***B***, Fluorescent photomicrograph of the same section illustrated in ***A*** showing the expression pattern of nsTub in the RMS and neuronal cell layers of the olfactory bulb. A large percentage of cells in the RMS and neuronal cell layers of the olfactory bulb express nsTub, a marker for immature neurons. Most cells within the RMS are believed to be neuronal-restricted progenitor cells (Menezes and Luskin, 1994; Menezes et al., 1995; Law et al., 1999; Temple and Alvarez-Buylla, 1999; Rochefort et al., 2002; Falls and Luskin, 2005). While migrating, these progenitors express proteins characteristic of immature neurons, and many remain mitotically active until they reach their postmigratory destination. ***C***, Fluorescent photomicrograph of the same section illustrated in ***A*** and ***B*** showing the expression pattern of p27 in the RMS and neuronal cell layers of the olfactory bulb. p27 is expressed throughout the RMS, particularly in the OBc. ***D–F***, High magnification of the region outlined by a box in ***B*** and ***C***. ***D***, Anti-nsTub staining. ***E***, Anti-p27 staining. ***F***, Merged image of ***D*** and ***E***. p27 is highly expressed in the OBc and in neuronal cell layers of the olfactory bulb (i.e., gcl and gl), where the neuronal cell marker nsTub also displays high expression levels. Scale bars: ***A–C***, 400 μm; ***D–F***, 100 μm. AOB, Accessory olfactory bulb; epl, external plexiform layer; mcl, mitral cell layer; OB, olfactory bulb; onl, olfactory nerve layer; LV, lateral ventricle; D, dorsal; A, anterior.

inducer of cell-cycle exit in neuronal progenitor cells of the SVZa and their progeny that migrate along the RMS into the olfactory bulb. We also demonstrate that functional inactivation of p27 in a KO mouse mutant prevents cell-cycle exit of neuronal progenitors, delays development of the gcl in the perinatal olfactory bulb, and promotes apoptotic cell death in this region. Finally, we show that p27^{KIP1} overexpression in cultured p27^{KIP1} null and wild-type (WT) SVZ cells reduced cell proliferation and self-renewal. Our data indicate that p27 plays an important functional role in the regulation of neuronal progenitor cell development during crucial phases of olfactory bulb growth.

Materials and Methods

Animals. The colony of WT mice and p27KO mice was generated from the same founders by isolating p27 and WT alleles. Genotypes of mice were determined by PCR analysis of tail DNA. Mice at P1, P7, and P14 were used in the present study. The plug day was regarded as E0. Birth

usually occurred on the 20th day of gestation. To normalize the ages of the animals examined, E20 was considered to be P0.

Preparation of sections. To analyze neural cell proliferation, animals were given intraperitoneal injections of 5-bromo-2′-deoxyuridine (BrdU; 200 mg/kg; catalog #B5002; Sigma) dissolved in 0.9% sodium chloride/7 mM NaOH 3 h before perfusion. P1 and P7 mouse pups were anesthetized by hypothermia, and P14 animals were anesthetized with two times the anesthetic dose of chloral hydrate (3% in 0.1 M PBS; catalog #C8383; Sigma). Animals were initially perfused transcardially with cold 0.1 M PBS (0.1 M sodium phosphate, 150 mM NaCl, pH 7.4), followed by 4% paraformaldehyde in 0.1 M PBS, pH 7.4. The brains, including the olfactory bulbs, were removed from the skull, postfixed at 4°C in the same fixative solution overnight, and cryoprotected with 30% sucrose. Tissues were embedded in O.C.T. (catalog #4583; Thermo Fisher Scientific) frozen with liquid nitrogen that was cooled with 2-methyl-butane. The brains were finally sectioned in the sagittal plane on a cryostat at 10 μm and mounted onto Superfrost Plus slides (catalog #48311-703; Thermo Fisher Scientific).

Immunohistochemistry. Sections containing the entire RMS were selected, and single- or double-labeled immunohistochemistry was performed. To expose the p27 and Ki67 antigen-binding epitopes (i.e., retrieval), the following procedure described by Tang et al. (2007) was used. Citrate buffer (0.01 M, pH 6.0) was preheated in a coplin jar in a 700 W microwave oven for 10 min at 30% power. Immediately after this preheating, slides were immersed in the hot (98°C) buffer. After 5 min, the solution (with slides) was reheated for 30 s at 30% power twice with a 5 min interval. After 16 min (5 min plus 30 s plus 5 min plus 30 s plus 5 min), the coplin jar was removed from the microwave, and the solution (with slides still immersed) was allowed to cool down to room temperature for 20 min. For BrdU staining, sections were immersed in 2N HCl at 40°C for 20 min to denature the DNA and rinsed twice with 40 mM borate buffer, pH 8.4, for 15 min to neutralize HCl. For p27/BrdU double labeling, the HCl treatment was first performed, followed by antigen retrieval. Slides were then processed for immunohistochemistry as described below.

Briefly, sections were washed in 0.1 M PBS, pH 7.4, for 30 min and kept in the blocking solution (2% normal goat serum in 0.3% Triton X-100/0.1 M PBS, pH 7.4) for 1 h. Subsequently, sections were incubated with primary antibodies at 4°C overnight. If tissue sections were stained with more than one antibody, this was done simultaneously. The antibodies used were as follows: mouse monoclonal p27 (1:200; catalog #610242; Transduction Laboratories, BD Biosciences) and rabbit monoclonal Ki67 (1:150; catalog #RM-9106-S0; NeoMarkers) to identify cells in the cell cycle; and rat monoclonal BrdU (2 μg/ml; catalog #ab6326-250; Abcam) to identify cells in S phase of the cell cycle. BrdU is a thymidine analog that is incorporated into DNA during the S phase of the cell cycle. Ki67 is a protein expressed during all active phases of the cell cycle, late G_1 to M phase, but is undetectable in quiescent cells (G_0 phase). Therefore, Ki67 represents an ideal marker to determine whether a given cell is in any phase of the cycle. Rabbit polyclonal neuron-specific type III β-tubulin (nsTub; 2.5 μg/ml; catalog #PRB-435P; Covance) and mouse monoclonal nsTub (1.25 μg/ml; catalog #G712A; Promega) were used to identify neurons, and mouse monoclonal neuronal nuclei (NeuN; 2 μg/ml; catalog #MAB377; Millipore Bioscience Research Reagents) to identify mature-terminally differentiated neurons. The following day, sections were rinsed with 0.1 M PBS and incubated with secondary antibodies, including goat anti-rat 488 (4 μg/ml; catalog #A11006; Invitrogen), goat anti-rat 568 (4 μg/ml; catalog #A11077), goat anti-mouse 488 (4 μg/ml; catalog #A11029), goat anti-mouse 568 (4 μg/ml; catalog #A11031), goat anti-rabbit 488 (4 μg/ml; catalog #A11008), and goat anti-rabbit 647 (4 μg/ml; catalog #A21245) counterstained with the fluorescent nuclear dye Hoechst 33342 (1 μg/ml; catalog #B2261; Sigma). After a 1 h incubation, sections were rinsed with 0.1 M PBS, pH 7.4, and coverslipped with Vectashield (catalog #H-1000; Vector Laboratories). In some experiments, the adjacent slides were counterstained with SYTO 24 (0.5 μM; catalog #S-7559; Invitrogen), and the number of SYTO 24-labeled cells was counted to determine the number of total cells.

p27(+) and BrdU(+) cell quantification. Sections containing the entire RMS (two sections per animal; three animals of each genotype at each age) were examined with a Zeiss Axioplan equipped with an LSM 510 confocal system. Laser scanning at 488 nm to image nsTub(+) cells, and at 543 nm to image BrdU(+) or p27(+) cells, was performed sequentially to avoid bleed-through of the fluorescent signals. For sections of P1 and P7 mice, three fields were taken of each chosen region [SVZa, vertical limb (vl), horizontal limb (hl), and core of olfactory bulb (OBc) of the RMS, and the gcl and gl of the olfactory bulb] using a 100× oil lens of a confocal microscope. Because the SVZa is reduced in size at P14, two rather than three fields were taken in this region.

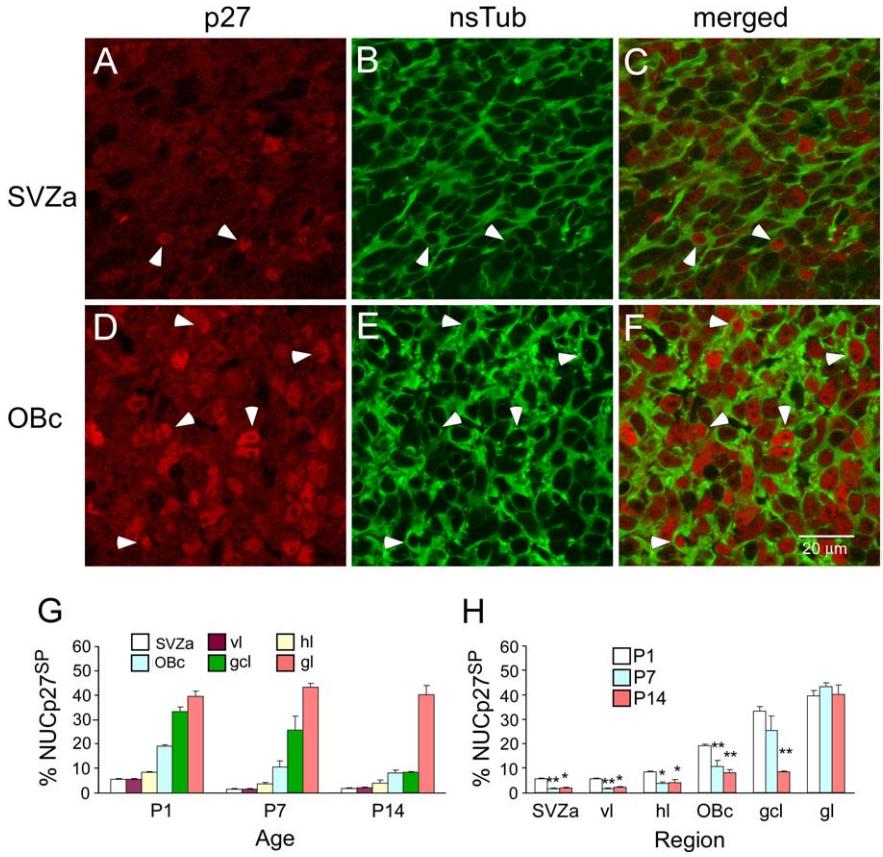

Figure 2. The percentage of cells displaying strong nuclear p27 expression increases from the SVZa to the OBc and is highest in the granule cell and glomerular layers of the olfactory bulb. ***A–F***, Representative photomicrographs of the SVZa (***A–C***) and OBc (***D–F***) stained for anti-p27 and anti-nsTub. A low number of RMS cells in the SVZa are NUCp27^{SP}, whereas more RMS cells in the OBc are NUCp27^{SP}. Arrowheads point to examples of identical NUCp27^{SP} cells. p27^{SP} nuclei (***A***, ***D***) are surrounded by nsTub(+) cytoplasm (***B***, ***E***), indicating that these are NUCp27^{SP}/nsTub double-labeled cells (***C***, ***F***). ***G***, Histogram of the percentage of NUCp27^{SP} cells shows an increasing gradient of expression from the SVZa to the neuronal cell layers of the olfactory bulb. ***H***, Histogram showing NUCp27^{SP} cells is significantly decreased at P7 and P14 in each subdivision of the RMS compared with the percentage at P1. There is no significant difference between P7 and P14 in any of the subdivisions of the RMS. For the gcl, this percentage is significantly decreased at P14 compared with P1. No significant difference is observed in the gl between the three ages. Error bars represent SEM. $*p < 0.05$; $**p < 0.01$.

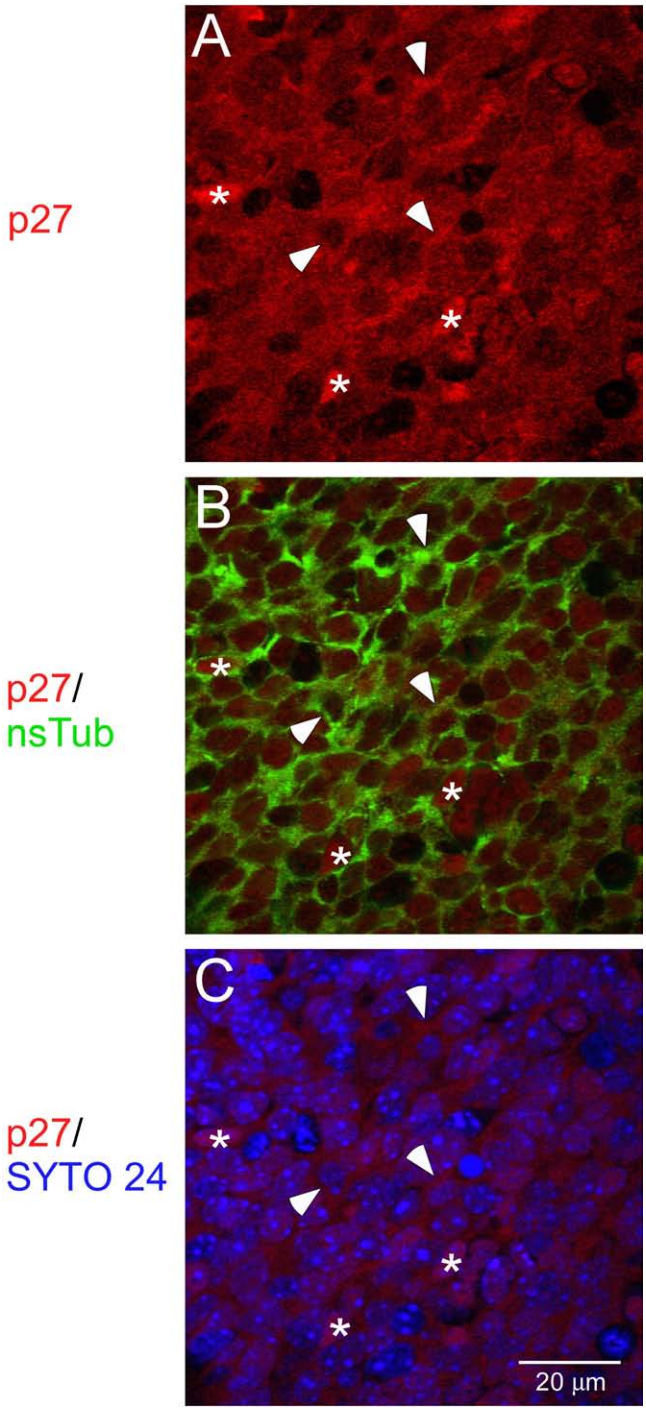

Figure 3. Subcellular distribution of p27 in the SVZa at P1. Photomicrographs of an identical section of the SVZa stained with antibodies to p27 (***A***), p27 and nsTub (***B***), and p27 and SYTO 24 (***C***) are shown. ***A***, Photomicrograph showing large numbers of p27(+) cells (red) in the SVZa. ***B***, Photomicrograph of the distribution of p27(+) (red) and nsTub(+) (green) cells. p27 (red) is localized both in the nucleus and/or in the cytoplasm (green; stained by nsTub). ***C***, Distribution of p27(+) cells in relation to SYTO 24(+) nuclei. The p27(+) nuclei (red) overlap with the SYTO 24 (blue) nuclei. Asterisks in the middle of p27(+) nuclei and arrowheads point to examples of p27(+) cytoplasmic cells at P1. Scale bar, 20 μm.

Quantification of positive cells was performed on files obtained from confocal images. To count cells with strong nuclear p27 staining (NUCp27^{SP}), images were processed with Photoshop 6.0, and the number of NUCp27^{SP} cells was counted by an observer who was blind to the ages and genotypes of the animals (Miyazawa et al., 2000). ImageJ software was used to count the SYTO 24(+) cell number (total cells) and to measure the scored area. The density of NUCp27^{SP} cells was calculated from the total number of NUCp27^{SP} cells divided by the total scored area. The total cell density was calculated by the number of SYTO 24(+) cells divided by the scored area. The percentage of NUCp27^{SP} cells was calculated by dividing the density of the positive cells by the total cell density. The quantification of BrdU(+) cells was also based on the confocal microscope files, and it was performed following the same procedure as described above. All the data are presented as mean ± SEM. Statistical analysis was performed using two-way repeated ANOVA and the *post hoc* Tukey's test.

Measurement of the thickness of RMS. Sections containing the entire RMS were selected and counterstained with the nuclear dye Hoechst. The thickness of hl of the RMS was used to represent the thickness of RMS. The hl displays an even diameter in a short segment immediately after the elbow of the RMS, before merging into the olfactory bulb. Images were taken of the hl using a Zeiss Axioscope fluorescence microscope equipped with a QImaging Retiga 1300 monochrome camera and processed with Canvas software. The thickness was measured using a micrometer by an observer blind to the genotypes and ages of the animals. Statistical analysis of data was performed using the two-way ANOVA and *post hoc* Tukey's test.

Measurement of thickness of gcl and NeuN(+) cell counting. NeuN immunostaining was performed on sections of the OBc. To measure the thickness of gcl and quantify the number of NeuN(+) cells, images of the gcl at the 11:00 position were taken with a Zeiss Axioscope fluorescence microscope (the tip of the olfactory bulb was taken as 12:00). A 200-μm-long straight line was drawn along the outer edge of gcl using Canvas software, and perpendicular lines were drawn from the two end points. To complete a rectangle, a line was drawn along the inner edge of the gcl parallel to the outer line. The width of this rectangle was regarded as the thickness of the gcl. The number of NeuN(+) cells in this rectangular zone was counted. The thickness of the gcl was measured using a micrometer. All these measurements were performed by an observer who was blind to the genotypes and ages of the animals. Statistical analysis of data was performed using the two-way ANOVA and *post hoc* Tukey's test.

Programmed cell death. To quantify apoptotic cell number and determine the phenotype of apoptotic cells, nsTub/terminal deoxynucleotidyl transferase (TdT)-mediated dUTP biotin nick-end double labeling (TUNEL) was performed based on protocols described previously by Doetsch et al. (2002) and Bauer et al. (2003), with some modification. Briefly, sections were first immunostained for nsTub. On the second day, sections were washed for 30 min after secondary antibody incubation. Subsequently, sections were incubated in TdT buffer [30 mM Tris-HCl, pH 7.5, containing 140 mM sodium cacodylate (catalog #C-0250; Sigma) and 1 mM $CoCl_2$ (catalog #C-3169; Sigma)] for 5–10 min. Subsequently, 0.06 nmol of biotin-16-dUTP (catalog #11388908910; Roche) and 24 U of TdT (catalog #03333 574001; Roche) were applied to every section and incubated for 1 h at 37°C, followed by a 15 min rinse at room temperature in TB buffer [300 mM NaCl (catalog #S271-3; Thermo Fisher Scientific) 30 mM sodium citrate (catalog #S-4641; Sigma)] to inactivate the enzyme. After a 5 min rinse in 0.1 M PBS, pH 7.4, sections were blocked with 10% normal goat serum in 0.3% Triton X-100/0.1 M PBS, pH 7.4, for 1 h and incubated with Alexa 568-conjugated streptavidin (2 μg/ml; catalog #S-11226; Invitrogen) for 1 h at room temperature. After a distilled water wash, sections were coverslipped with Vectashield. Negative control sections were processed with the same protocol, except for omission of the incubation with TdT. Before TdT buffer incubation, positive control sections were incubated with DNase I (grade II, 500 U/ml in 50 mM Tris-HCl, pH 7.5; catalog #10-104-159-001; Roche) for 10 min at room temperature and rinsed with PBS for 15 min. TUNEL(+) cells in the whole RMS and gcl were counted by an observer who was blind to the genotypes and ages of the animals, and the scored areas of the whole RMS and gcl were calculated with Canvas software. The density of TUNEL(+) cells was determined by using the total TUNEL(+) cell number divided by the scored area. Statistical analysis of the data was performed using two-way ANOVA and the *post hoc* Tukey's test.

Neurosphere cultures. P1 WT and p27KO mice were used to dissect out the SVZ. The SVZ tissue was digested for 30 min at 37°C in HBSS (catalog #14170-161; Invitrogen) containing papain (13 U/ml; catalog #T4762;

Sigma), DNase (5 U/ml; catalog #D5427; Sigma), and trypsin (0.1%; catalog #T4799; Sigma). Single cells were cultured for neural stem cell colony-forming (neurosphere) assays (Reynolds and Weiss, 1992; Jablonska et al., 2007) at 10 cells per microliter on uncoated 24-well plates (BD Falcon) and grown for 6 d *in vitro* in stem cell medium [DMEM/F-12 containing 1× B27 and 1× N2 (both from Invitrogen), with a daily addition of epidermal growth factor (EGF; 20 ng/ml) and basic FGF (10 ng/ml) (both from Millipore; catalog #01-407 and #01-114, respectively)] (Jablonska et al., 2007). Neurospheres formed from WT and p27KO cell suspensions were counted and repassaged for secondary and tertiary neurosphere formation.

Viral infection. For p27-rescue experiments in p27KO neural progenitor cells (NPCs), we performed gene delivery experiments by using a retroviral infection system. Dissociated NPCs from WT and p27KO mice were plated at 10 cells per microliter, and from day 1 cells were infected with a mock or a p27 retrovirus (10^9 CPU). For analysis of cell proliferation and cell survival after retroviral infection, cell cultures were maintained under conditions that stimulated cell proliferation (DMEM/F-12 containing 10 ng/ml EGF and FGF each) for 7 d and processed for immunocytochemistry. Cell quantification for each condition and each cell type (WT-mock, WT-p27 virus, KO-mock, KO-p27 virus) was performed on at least six to nine samples obtained from two to three different culture experiments. The results are presented as mean ± SEM. The *t* test was performed to establish statistical significance.

Immunocytochemistry. For immunocytochemistry, cell cultures were processed after 7 d *in vitro* (Aguirre and Gallo, 2004). Immunostaining was performed with anti-Ki67 (catalog #NCL-Ki67p; Novocastra) and anti-activated Caspase 3 (catalog #9661; Cell Signaling Technology).

Western blot analysis. For protein extraction, SVZ tissue obtained from P1 WT and p27KO mouse brains was homogenized in RIPA-Lysis buffer (catalog #SC24948; Santa Cruz Biotechnology) containing proteases inhibitors (Jablonska et al., 2007). Protein concentration was determined in each sample, and the same protein amount (25 μg) was separated on polyacrylamide gels. Proteins were transferred to polyvinylidene fluoride membranes (catalog #TM151-1; Millipore), and the specific bands were detected using an enhanced chemiluminescence substrate mixture. To quantify the relative levels of cell-cycle proteins, x-ray films were scanned using an Agfa T1200 scanner with Photolook software. Protein levels were normalized to actin and expressed as arbitrary units for each condition. Cell-cycle protein levels were compared between WT and p27KO mice. The following antibodies (all from Santa Cruz Biotechnology) were used: anti-CDK2 (catalog #SC6248), CDK4 (catalog #SC260), CDK6 (catalog #SC177), cyclin D (catalog #SC450), cyclin E (catalog #SC481), p21 (catalog #SC6246), p27 (catalog #SC776), retinoblastoma (Rb; catalog #SC7905), pRb (Ser780; catalog #SC12901), and pRb(Ser807; catalog #SC16670). Anti-actin was from Millipore Bioscience Research Reagents (catalog #MAB1501R).

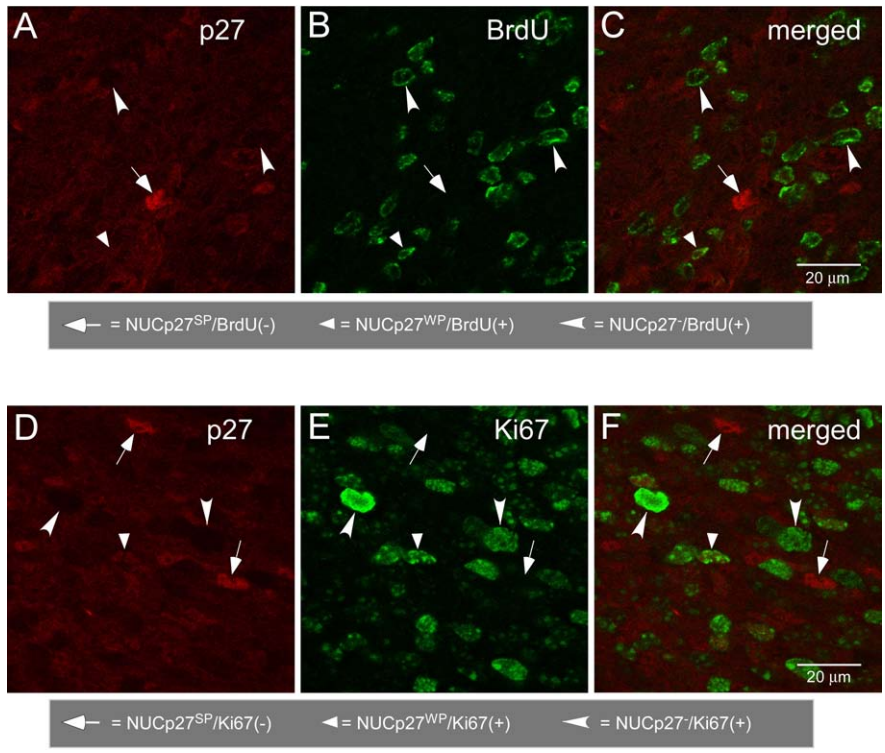

Figure 4. NUCp27^{SP} cells are negative for the cell proliferation markers BrdU and Ki67. ***A–C***, Fluorescent photomicrographs of identical fields showing that in the SVZa at P1, NUCp27^{SP}(+) cells are negative for BrdU, and only NUCp27^{WP}(+) or NUCp27^{-} cells are BrdU(+). ***D–F***, Fluorescent photomicrographs of identical fields showing that NUCp27^{SP}(+) cells are not labeled with Ki67 and only NUCp27^{WP}(+) or NUCp27^{-} are Ki67(+). Scale bars, 20 μm.

Results

p27 expression pattern in the RMS and neuronal cell layers of the olfactory bulb

SVZa-derived neuronal progenitor cells migrate along the RMS toward the olfactory bulb. Figure 1*A* shows a parasagittal section of a P1 WT mouse stained with the nuclear marker Hoechst to show the high density of cells in the RMS. During the early postnatal period, SVZa-derived neuronal progenitor cells are the major type of cells in the neonatal and early postnatal RMS, which can be well labeled by nsTub (Menezes and Luskin, 1994; Law et al., 1999; Falls and Luskin, 2006) (Fig. 1*B*,*D*). To define a possible role of p27 in the regulation of cell proliferation and survival in the RMS and olfactory bulb, we first used immunohistochemistry to determine its expression pattern in these regions in P1, P7, and P14 mice. We observed that, in WT mice, p27 is ubiquitously expressed in the RMS and the olfactory bulb (Fig. 1*C*,*E*). Many intensely labeled cells could be seen in the OBc, in the rostral segment of the RMS, and in neuronal cell layers of the olfactory bulb (Fig. 1*C*,*E*). Most, if not all, of the p27(+) cells were double labeled with the neuronal marker nsTub (Fig. 1*B*,*D*,*F*). No p27 expression was detected in the SVZa, RMS, or OB of p27KO mice (supplemental Fig. 1, available at www.jneurosci.org as supplemental material, and data not shown).

Based on the visual assessment of nuclear p27 label intensity, we classified cells as nuclear p27 negative (NUCp27^{-}), nuclear p27 weakly positive (NUCp27^{WP}), and nuclear p27 strongly positive (NUCp27^{SP}) (Fig. 2*A–F*). We found that the vast majority of nsTub(+) cells are also p27(+). In the SVZa, few nsTub(+) cells are also NUCp27^{SP} (Fig. 2*A–C*). Compared with the SVZa, more nsTub(+) cells are NUCp27^{SP} in the OBc (Fig. 2*D–F*). To quantitatively analyze the expression pattern of p27, we scored the number of NUCp27^{SP} cells in the SVZa, vl, hl, and OBc of the RMS and in the gcl and gl of the olfactory bulb. At each age, the percentage of NUCp27^{SP} cells showed a gradient from the SVZa (initial segment of the RMS) to the neuronal cell layers of the olfactory bulb, with the lowest percentage in the SVZa and the highest in the gl (caudal^{low}–rostral^{high} gradient) (Fig. 2*G*). When compared with P1, the percentage of NUCp27^{SP} cells in each

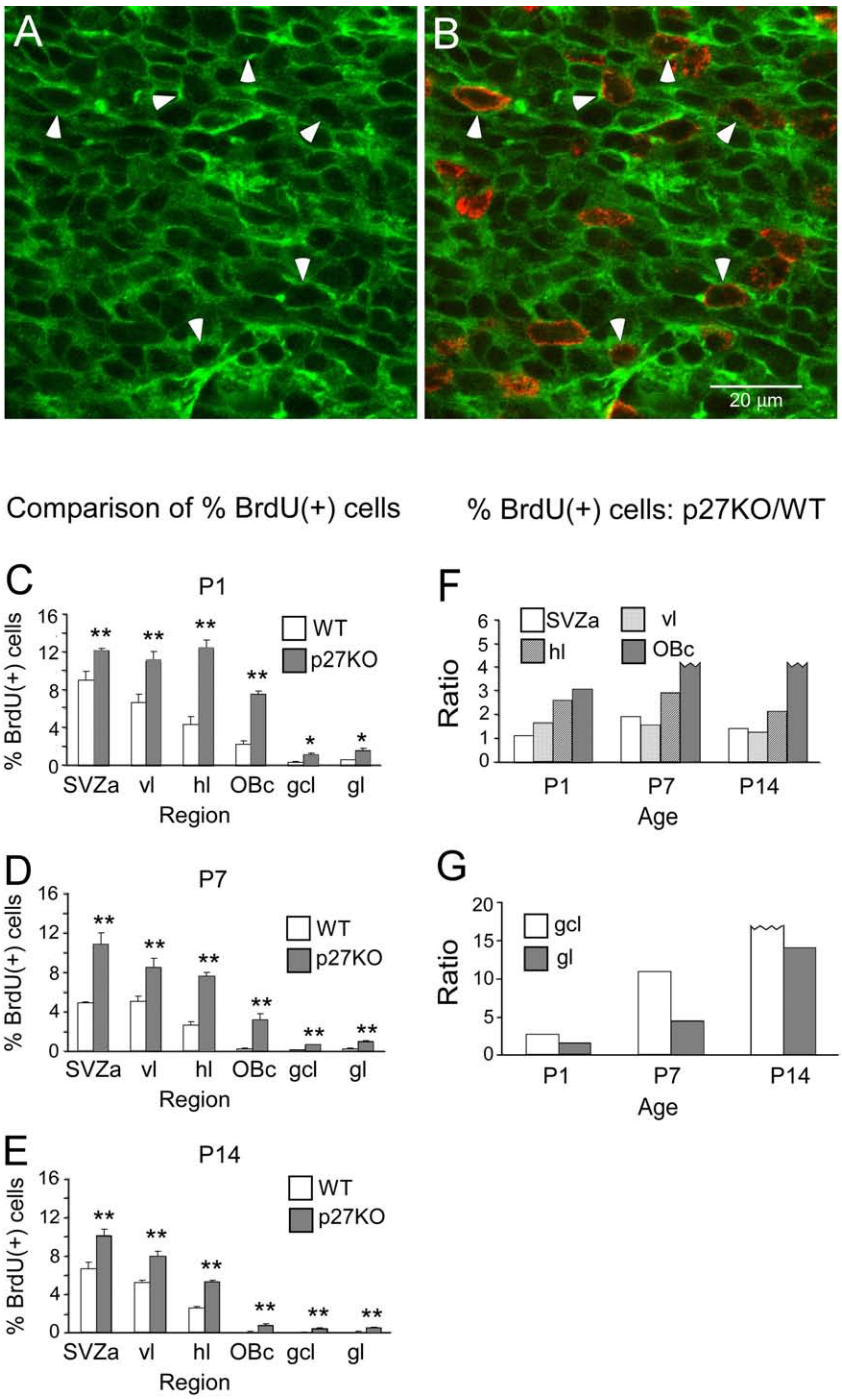

Figure 5. The percentage of BrdU(+) cells in the RMS and olfactory bulb is higher in p27KO mice compared with WT mice. ***A***, ***B***, Representative fluorescent photomicrographs of identical fields showing that some BrdU(+) cells in the RMS (***B***) are also labeled with nsTub (***A***), suggesting that these cells are neuronal progenitor cells. Arrowheads point to examples of BrdU(+) nsTub(+) cells at P1. Scale bar, 20 μm. ***C–E***, Comparison between BrdU(+) cells in WT and p27KO animals at P1, P7, and P14. ***C***, At P1, the percentage of BrdU(+) cells is significantly higher in p27KO mice compared with WT mice. In WT mice, BrdU(+) cells display a well developed gradient from the SVZa to the OBc and neuronal cell layers of the olfactory bulb. ***D***, At P7, the percentage of BrdU(+) cells is significantly higher in p27KO mice compared with WT mice. Both genotypes exhibit a gradient from the SVZa to the OBc and neuronal cell layers of the olfactory bulb. ***E***, At P14, the percentage of BrdU(+) cells is significantly higher in p27KO mice compared with WT mice. ***F–G***, The ratio between the percentages of BrdU(+) cells in p27KO versus WT mice in the caudal–rostral extent of the RMS and neuronal layers of the olfactory bulb during postnatal development. *$p < 0.05$; **$p < 0.01$.

region was significantly lower at P7 and P14, except for the gl, but it did not show significant difference between P7 and P14 in each region (Fig. 2*H*). These data indicate that p27 displays a spatiotemporal pattern of expression in the RMS and olfactory bulb.

We also investigated the subcellular localization of p27. From P1 to P14, nsTub antibody labels the cytoplasm of neuronal progenitor cells in the RMS and olfactory bulb, therefore we performed nsTub/p27 double labeling counterstained with SYTO 24. It was found that p27 not only distributes in the cytoplasm but also localizes in the nucleus (Fig. 3). These data suggest that p27 might have different functions in the RMS and neuronal cell layers of the olfactory bulb according to its subcellular locations (Besson et al., 2004; Nguyen et al., 2006; Reiner and Sapir, 2006).

p27 inhibits cell proliferation in the RMS and olfactory bulb

To assign a role to p27 in the regulation of cell proliferation in the RMS and olfactory bulb, we first performed double labeling with anti-p27 and markers of cell proliferation (i.e., BrdU and Ki67). We observed that from P1 to P14, NUCp27^{SP} cells were consistently negative for BrdU and Ki67 but NUCp27^{-} and NUCp27^{WP} cells expressed detectable BrdU and Ki67 (Fig. 4). These data indicate that high levels of nuclear p27 expression likely induce cells to withdraw from the cell cycle.

To directly address whether p27 inhibits its cell proliferation, we compared the percentage of BrdU(+) cells between WT mice and p27KO mice. In WT mice, we observed that some BrdU(+) nuclei (Fig. 5*B*) were surrounded by nsTub-labeled cytoplasm (Fig. 5*A*), indicating that these proliferating cells are neuronal progenitors. Given the time span after BrdU injection (3 h), these BrdU(+) cells are likely in S or G_2 phase of the cell cycle. Furthermore, in cultured SVZa progenitor cells, some nsTub(+) cells were also labeled with phospho-Histone H3, a marker for M phase (supplemental Fig. 2, available at www.jneurosci.org as supplemental material).

We quantitatively scored the percentage of BrdU(+) cells in the RMS and neuronal cell layers of the olfactory bulb. In WT mice, we observed that BrdU(+) cells displayed a caudal^{high}–rostral^{low} gradient at each age analyzed (P1, P7, P14), which was in contrast with the gradient of p27 expression (Fig. 5*C–E*). We also found that, from P1 to P14, the percentage of BrdU(+) cells was significantly higher in p27KO mice compared with WT mice in all regions analyzed (Fig. 5*C–E*). At P1, WT mice exhibited a well developed BrdU labeling gradient (Fig. 5*C*) that was absent in p27KO mice (SVZa ≈ vl ≈ hl; slight decrease in OBc). Importantly, although proliferation in the SVZa of WT mice declined from P1 to P7 and P14 (≈ 50%), the percentage of BrdU(+) in p27KO mice showed

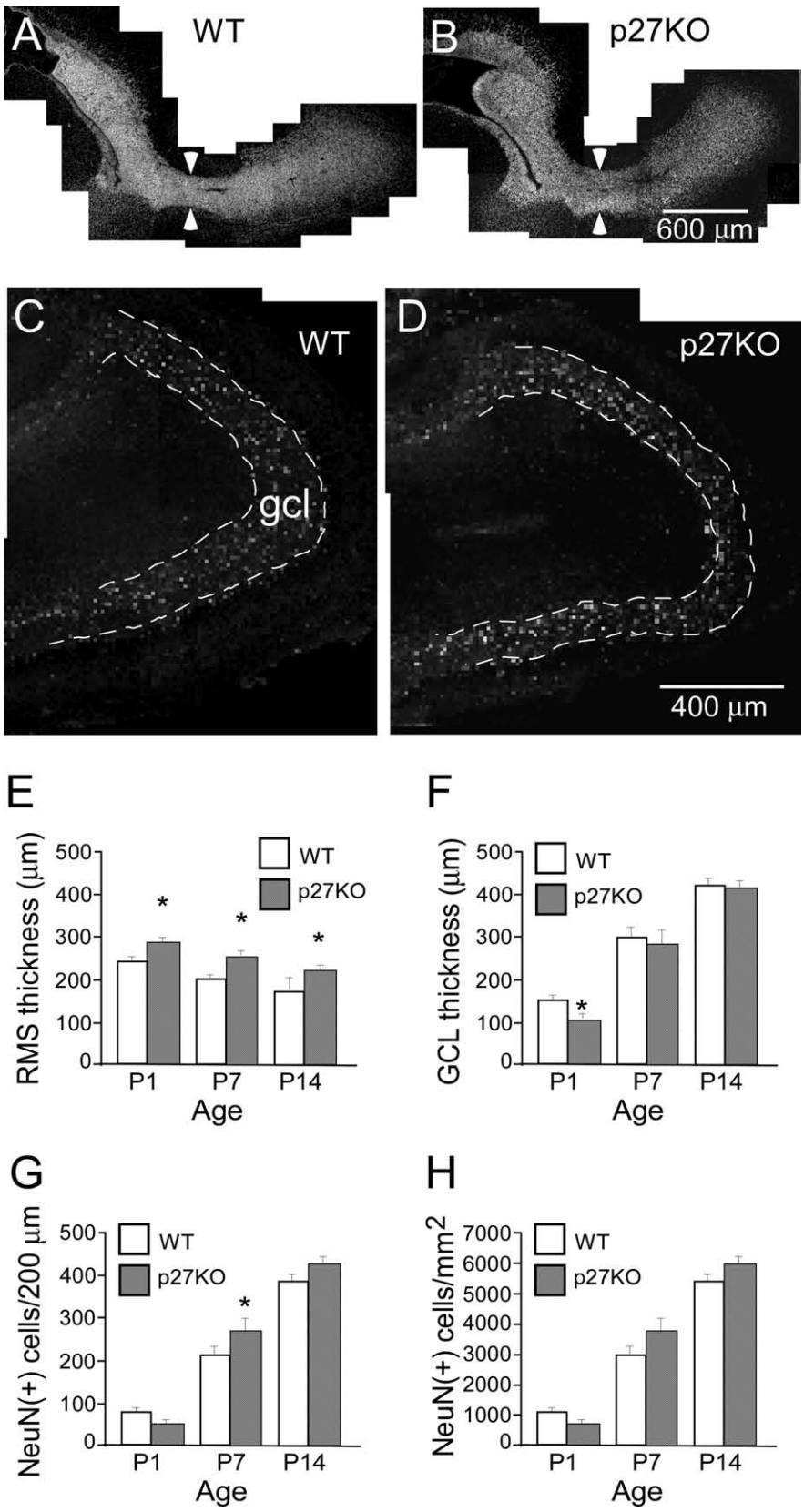

Figure 6. p27 deletion leads to an increase in RMS thickness and a delay in development of the gcl of the olfactory bulb. ***A***, ***B***, Fluorescent photomicrographs showing staining of the nuclear dye Hoechst 33342 in parasagittal sections of the RMS in the P1 WT (***A***) and p27KO (***B***) mice. Arrowheads point to the location where the thickness of RMS was measured in the hl of the RMS. Scale bar, 400 μm. ***C***, ***D***, Bright-field photomicrographs of NeuN staining showing that at P1 the olfactory bulb gcl is thinner in p27KO mice (***D***) compared with WT mice (***C***). Dashed lines outline the gcl. Scale bar, 400 μm. ***E***, ***F***, Quantitative comparison of the thickness of the RMS and gcl of olfactory bulb between WT and p27KO mice. ***E***, The RMS thickness is significantly larger in the p27KO mice compared with WT mice at all ages analyzed. $*p < 0.05$. ***F***, At P1, the thickness of the gcl is significantly thinner in p27KO mice than in WT mice. $*p < 0.05$. ***G***, The number of NeuN(+) cells per 200 μm in the RMS. At P1, the number of NeuN(+) cells per 200 μm length appears to be lower in p27KO mice than in WT mice, although not significantly different. At P7, the number of NeuN(+) cells is significantly higher in p27KO mice than in WT mice. At P14, the number of NeuN(+) cells appears to be higher in p27KO mice than in WT mice, although not significantly different. $*p < 0.05$. ***H***, The graph shows that there is not a significant difference in the NeuN(+) cell density in the gcl between the genotypes at any of the ages quantitatively analyzed.

little change. Finally, despite the fact that cell proliferation in p27KO mice remained higher than in WT mice from P1 to P14, the p27KO mice displayed a progressively steeper gradient with increasing age (Fig. 5*C–E*).

To further assess the role of p27 in inhibiting cell proliferation, we analyzed the ratio of the percentage of BrdU(+) cells between p27KO and WT mice. This ratio displayed a trend toward higher values from SVZa to the OBc (particularly high in the OBc) (Fig. 5*F*,*G*), suggesting that the contribution of p27 to inhibition of cell proliferation increases as cells migrate from the SVZa to the OBc. This finding is consistent with the spatial expression pattern of p27 shown in Figure 2. However, even in p27KO mice, the proliferation rate in OBc was much lower than in the SVZa, and proliferation decreased with increasing age, indicating an important role of other factors in controlling the cell proliferation rate. At all ages studied, the proliferation rate was also higher in target layers of the olfactory bulb (gcl, gl) of p27KO mice compared with WT mice. At P14, proliferation persists in these neuronal layers of p27KO mice, but it was almost undetectable in WT mice. Altogether, these data indicate that SVZa-derived neuronal progenitor cells can proliferate *in vivo* and *in vitro* and p27 inhibits the proliferation of cells in the RMS and olfactory bulb.

The RMS size is increased in the p27KO mouse

To determine whether the changes in cell proliferation observed in the p27KO mice affected the size of the RMS, we measured the thickness of RMS in the hl of the RMS. We consider the thickness of the hl as representative of the thickness of RMS, because the hl displays a consistent diameter in a short segment immediately after the elbow, before merging into the OBc. Figure 6, *A* and *B*, shows

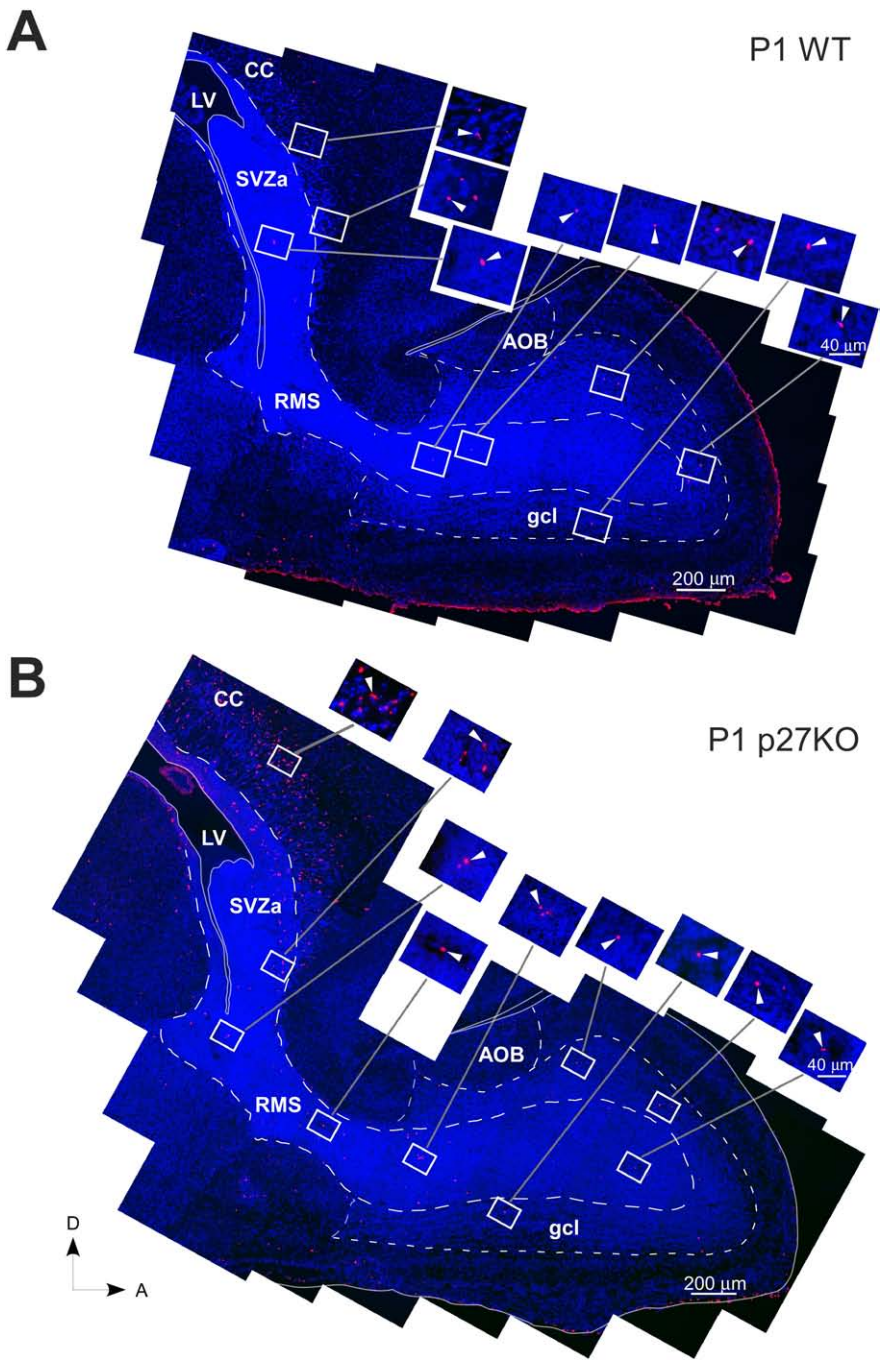

Figure 7. Deletion of p27 causes an increase in the apoptotic cell death in the RMS and gcl of the olfactory bulb. Photomontages of sagittal sections of the P1 forebrain of a WT (***A***) and p27KO (***B***) mouse illustrating the distribution of cell nuclei stained with DAPI (4′,6-diamidino-2-phenylindole; blue) and apoptotic cells stained with TUNEL (red) along and flanking the RMS to the anterior end of the olfactory bulb. The insets are magnifications of each box shown in the photomontages. The arrowheads in the insets point to representative TUNEL(+) (red) cells. The RMS is outlined by large dashed lines. The gcl and AOB are outlined by small dashed lines. The lateral ventricle and its extensions into the RMS are outlined by thin white lines. A thin white line also outlines the olfactory bulb and forebrain. A, Anterior; AOB, accessory olfactory bulb; CC, corpus callosum; D, dorsal; LV, lateral ventricle. Scale bars: ***A***, ***B***, 200 μm; insets, 40 μm.

the RMS of P1 WT and p27KO mice, respectively. At all ages tested, the diameter of the hl was significantly larger (~20%) in p27KO mice than that in WT mice (Fig. 6*E*). These data strongly suggest that a higher cell proliferation rate in the RMS contributes to an increase in its size.

Development of the neuronal cell layers of the olfactory bulb is delayed in the p27KO mouse

We also investigated whether the development of the olfactory bulb was affected in p27KO mice by comparing the thickness of the gcl and the number of neurons in WT and p27KO mice. Given that SVZa-derived neuronal progenitor cells will become postmitotic when they reach the gcl, we labeled sections with the mature neuronal marker NeuN to visualize the gcl. Figure 6, *C* and *D*, shows a photomontage of the P1 gcl in the WT and p27KO mouse, respectively. By taking the tip of the olfactory bulb as 12:00, we found that at the 11:00 position the thickness of the gcl was significantly decreased (~25%) in p27KO mice compared with WT mice. Conversely, only nonsignificant differences were observed at P7 or P14 (Fig. 6*F*). We then counted the number of NeuN(+) cells in the gcl in the two genotypes. At P1, the number of NeuN(+) cells was reduced in p27KO versus WT mice, although this difference was not significant. In contrast, at P7 the number was significantly higher in p27KO mice than in WT mice (Fig. 6*G*). At P14, this trend continued, although differences were not significant (Fig. 6*G*).

The differences in the number of NeuN(+) cells observed between p27KO and WT mice could be attributable to the decrease in thickness of the gcl, therefore we also quantified the density of NeuN(+) cells in this region. We observed that cell density did not significantly change between genotypes at any age analyzed (Fig. 6*H*). These data indicate that development of the gcl was delayed at P1, but this was not caused by a delay in neuronal cell differentiation.

p27 plays a role in cell survival in the RMS

To study whether cell survival was affected in p27KO mice, we performed TUNEL labeling as a marker of cells undergoing cell death at different developmental stages. The number of TUNEL(+) cells was counted, and the density of TUNEL(+) cells was determined in the entire RMS and gcl.

Figure 7 and supplemental Figure 3*A–D* (available at www.jneurosci.org as supplemental material) show that, in both genotypes and at all ages, we observed that TUNEL(+) cells distributed randomly and did not display an apparent gradient. No more TUNEL(+) cells were found in the SVZa, where a higher cell proliferation index was found (Fig. 5) compared with other regions (Fig. 7; supplemental Fig. 3, available at www.jneurosci.org as supplemental material).

To determine the phenotype of TUNEL(+) cells, we per-

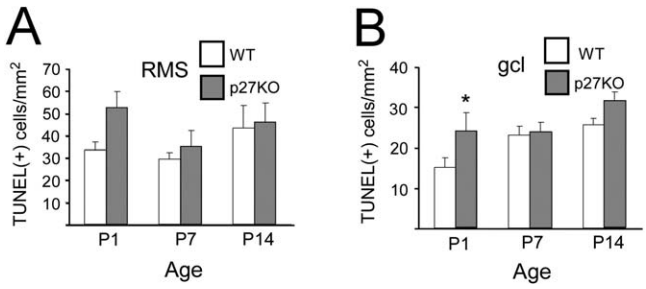

Figure 8. Quantitative comparison of TUNEL(+) cells in the RMS and gcl in WT and p27KO mice. Histograms show the comparison of TUNEL(+) cells in the RMS (***A***) and gcl (***B***) in WT (white bars) and p27KO (hatched bars) mice at P1, P7, and P14. At all ages, in the RMS more cells are TUNEL(+) in p27KO mice compared with WT mice, although the difference is not significant. ***B***, At P1, however, significantly more cells are TUNEL(+) in the gcl of p27KO mice compared with WT. $*p < 0.05$.

formed nsTub/TUNEL double labeling. Consistent with previous reports (Doetsch et al., 2002; Moreno-Lopez et al., 2004), at P1 a small percentage of TUNEL(+) cells were also nsTub(+) (data not shown), and the majority of TUNEL(+) cells were not labeled with nsTub. At this age, the density of TUNEL(+) cells was higher in the RMS of p27KO than in WT mice (Fig. 8*A*). At P7 and P14, the density of TUNEL(+) cells in the RMS did not show significant differences between p27KO and WT mice (Fig. 8*A*). Finally, at P1, the density of TUNEL(+) cells in the gcl was significantly higher in p27KO mice than in WT mice, but it was not significantly different at P7 and P14 (Fig. 8*B*). These data indicate that increased apoptosis contributes to the delay in the development of the gcl in P1 p27KO mice. Because the RMS also contains other progenitor cell populations during the first and second postnatal week, we believe that a percentage of the TUNEL(+) cells at P7 and P14 might be NG2-expressing cells or their progeny (Aguirre and Gallo, 2004).

Role of p27 in SVZ progenitor/stem cell proliferation and self-renewal

To determine whether the phenotype observed in p27KO SVZ progenitors *in vivo* was also reproduced *in vitro*, we analyzed the proliferation potential of NPCs of the WT and p27KO mouse SVZ by neurosphere formation assays. The number of neurospheres was determined after three successive passages (7 d each) of NPCs from p27KO and WT mice. Throughout all three passages, the number of neurospheres calculated per 10,000 seeded cells was significantly higher in the p27KO than in WT mice (Fig. 9*A*,*D*,*G*). Infection of a p27 retrovirus in both groups of cells significantly diminished the number of formed neurospheres in the second and third passage compared with cells infected with a mock retrovirus (Fig. 9*B*,*C*,*E*,*F*,*H*,*I*). The effects of the retrovirus on neurosphere formation were more pronounced in p27KO cells than in WT cells (Fig. 9*C*,*F*,*H*,*I*).

To determine the proliferation rate in p27KO and WT NPCs after retroviral infection, we immunolabeled cultured cells or neurospheres with anti-Ki67 antibody. Both in p27KO and WT cultures, the rate of proliferation was significantly reduced after retroviral infection compared with cells infected with a mock retrovirus (Fig. 10*A*,*B*,*E*,*F*,*I*). Caspase 3 immunostaining was also used to determine whether p27 overexpression enhanced cell apoptosis. After infection with the p27 retrovirus, apoptosis increased by ~6-fold in p27KO cells and by 1.5-fold in WT cells (Fig. 10*C*,*D*,*G*,*H*,*J*).

To gain further insight into the molecular mechanism(s) underlying the involvement of p27 in SVZ cell proliferation, we analyzed expression of a number of cell-cycle regulatory proteins, including the following: (1) the cyclin-dependent kinases CDK2, CDK4, and CDK6; (2) their activators cyclin D and cyclin E; (3) the other inhibitor $p21^{Cip1}$; and (4) their phosphorylated substrates: Rb-total, p-Rb(Ser780), p-Rb(Ser807). Western blot analysis was performed in WT and p27KO SVZ protein extracts from P1 mice. Figure 11 shows that, in p27KO SVZ tissue, expression of CDK2, Rb-total, p-Rb(Ser780), and p-Rb(Ser807) was upregulated compared with WT. Conversely, expression of p21 was reduced in p27KO SVZ compared with WT.

Altogether, these results indicate that p27 plays an important role in regulating NPC proliferation in the SVZ and strongly suggest that the CDK2–Rb pathway is engaged in maintaining proliferation of this progenitor cell population.

Discussion

In this study, we determined the spatiotemporal expression pattern of p27 in the RMS and in neuronal cell layers of the olfactory bulb. Spatially, the expression of p27 increases from the SVZa to the olfactory bulb, similar to the p19 expression pattern (Coskun and Luskin, 2002), although the increase observed in p27 shifted more rostrally. Temporally, the expression of p27 at P1 is higher than that at P7 and P14, consistent with a previous study showing a decreasing mRNA expression of p27 in the RMS with age (van Lookeren Campagne and Gill, 1998). Concerning p27 in the neuronal cell layers of the olfactory bulb, its expression decreases with age in the gcl but increases in the gl. Collectively, these findings support the notion that the interneurons in the gcl and gl may be different neuronal subtypes (Smith and Luskin, 1998; Hack et al., 2005; Kohwi et al., 2005; Lemasson et al., 2005) and that p27, as well as the other cell-cycle inhibitor p19, plays different roles in these interneurons, such as regulation of cell-cycle exit or maintenance of cellular quiescence (Legrier et al., 2001).

SVZa-derived neuronal progenitor cells migrate toward the olfactory bulb along the RMS, and differentiate into mature interneurons when they reach the olfactory bulb (Luskin, 1993; Lois and Alvarez-Buylla, 1994). These neuronal progenitor cells continue to divide during their migration (Menezes et al., 1995; Smith and Luskin, 1998; Law et al., 1999; Coskun and Luskin, 2002). Recent studies have shown that many factors, such as CDKI p19 (Coskun and Luskin, 2002), slit (Nguyen-Ba-Charvet et al., 2004), tenascin-R (Saghatelyan et al., 2004), and prokineticin 2 (Ng et al., 2005) are involved in the regulation of the proliferation, migration, and differentiation processes in this pathway. It has also been found that p27, a member of the CDKIs, regulates neural cell proliferation, migration, and differentiation in different brain regions, including the cerebellum (Miyazawa et al., 2000), retina (Levine et al., 2000; Cunningham et al., 2002), cerebral cortex (Zindy et al., 1999; Goto et al., 2004; Nguyen et al., 2006), adult subventricular zone (Doetsch et al., 2002), and olfactory epithelium (Legrier et al., 2001).

The function of p27 is closely related with its subcellular localization. The nuclear localization of this protein is a prerequisite for its inhibitory action on cell proliferation (Reynisdottir and Massague, 1997; Orend et al., 1998; Tomoda et al., 1999). In the nucleus, p27 inhibits the activity of cyclin E/A-CDK2 and prevents cell-cycle progression (Sherr and Roberts, 1995). Conversely, p27 is exported to the cytoplasm after phosphorylation in Thr 187 or Ser 10 (Rodier et al., 2001; Boehm et al., 2002). Cytoplasmic p27 decreases the level of nuclear p27, a regulatory step that is required for a cell to reenter the cycle, and promotes cell migration, as demonstrated in HepG2, fibroblasts, lung cancer

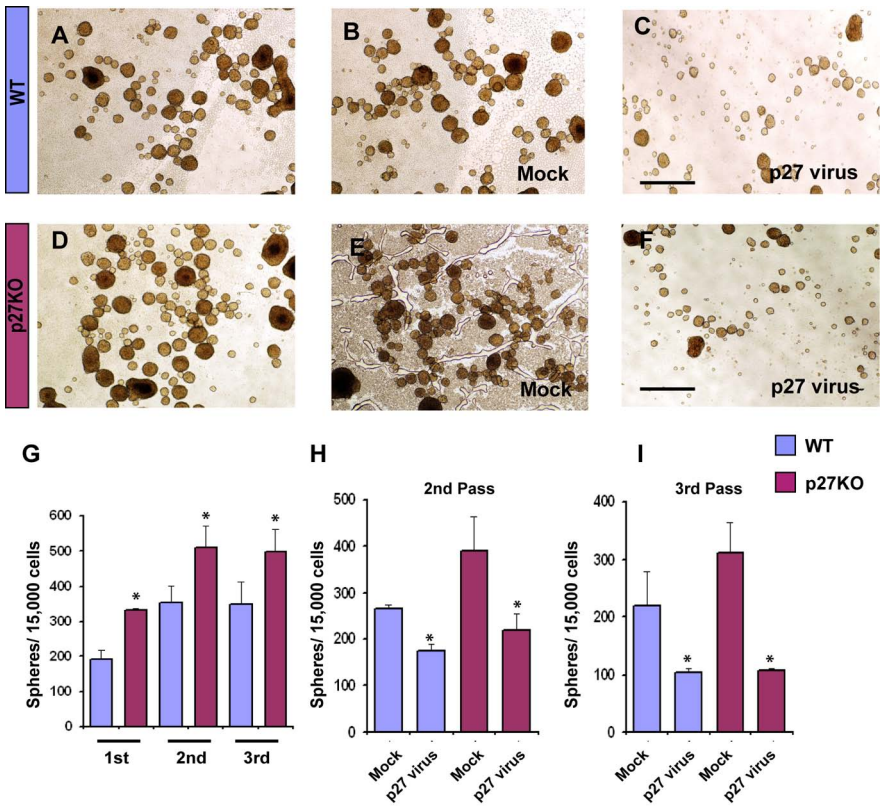

Figure 9. Overexpression of p27 reduces proliferation and self-renewal of NPCs of the SVZ. ***A–F***, SVZ neurospheres were obtained from single cell suspensions prepared from WT (***A–C***) and p27KO (***D–F***) mice at P1. To assess neural progenitor self-renewal potential, neurosphere numbers were counted after the first, second, and third passage, respectively. ***B***, ***C***, ***E***, ***F***, SVZ cells from P1 brains were first cultured and then infected with either a mock-retrovirus (***B***, ***E***) or p27-retrovirus (***C***, ***F***) to assay proliferation and self-renewal in SVZ cells of the WT and p27KO mice. Scale bars, 500 μm. ***G***, A higher number of neurospheres were found throughout all three passages in p27KO cultures compared with WT. ***H***, ***I***, At both second and third passage, WT and p27KO SVZ cell proliferation and self-renewal were reduced after p27 overexpression compared with mock-retrovirus. $^{*}p < 0.03$.

cells, mesengial cells, and neurons (McAllister et al., 2003; Assoian, 2004; Besson et al., 2004, 2006; Crean et al., 2006; Nguyen et al., 2006). Consistent with these findings, overexpression of cytoplasmic p27 caused an increase in cell motility (Wu et al., 2006).

More recently, several studies demonstrated that neurons express p27 both in the nucleus and cytoplasm (Kawauchi et al., 2006; Nguyen et al., 2006). Its effects on cell migration are thought to occur through the inhibition of RhoA activity and regulation of actin assembly (Besson et al., 2004; Nguyen et al., 2006). In the present study, we demonstrate that neuronal progenitor cells in the RMS and olfactory bulb express p27 in the nucleus and/or cytoplasm, strongly suggesting that p27 might regulate cell migration in the RMS. The finding that cytoplasmic p27 is reduced in the olfactory bulb compared with RMS is consistent with this hypothesis.

Many studies demonstrated that p27 inhibits the proliferation of different progenitor cell types in the retina (Levine et al., 2000; Cunningham et al., 2002), cerebellum (Miyazawa et al., 2000), and SVZ (Doetsch et al., 2002). Doetsch et al. (2002) found that, in the adult SVZa of the p27KO mouse, the number of neural stem cells did not change, but the pool of transit amplifying cells increased and neuroblast number decreased. Conversely, it was demonstrated that neurogenesis was enhanced in the cerebral cortex of the p27KO mouse (Goto et al., 2004) and that postmitotic neurons are able to reenter the cell cycle in p19/p27 double-KO mice (Zindy et al., 1999). These results suggest that the effects of p27 on cell proliferation in postnatal neurogenic regions of the brain are cell-type specific.

In our studies, we observed that the gradient of BrdU(+) cells (caudal^{high}–rostral^{low}) is the inverse of the expression pattern of p27 (caudal^{low}–rostral^{high}) in both WT and p27 (present study) and p19KO (V. Coskun and M. B. Luskin, unpublished observation) mice. Furthermore, the percentage of BrdU(+) cells was significantly increased in p27KO mice compared with WT mice. These data indicate that p27 inhibits cell proliferation in the RMS and olfactory bulb. We also found that NUCp27^{SP} cells are negative for cell-cycle markers, consistent with previous studies showing that cells accumulate p27 in the nucleus and exit the cell cycle when p27 levels reach a plateau (Durand et al., 1997; Miyazawa et al., 2000). Furthermore, the finding that cell proliferation in p27KO mice decreases with age and that cells successfully exit the cell cycle in the RMS and olfactory bulb indicates that p27 only partially contributes to regulate cell proliferation in these brain regions (Miyazawa et al., 2000), and some CDKs (van Lookeren Campagne and Gill, 1998; Padmanabhan et al., 1999) or CDKIs, such as p16 (Molofsky et al., 2006), p19 (Zindy et al., 1999; Coskun and Luskin, 2001; Cunningham et al., 2002), p21 (Siegenthaler and Miller, 2005), and p57 (Dyer and Cepko, 2001) are involved in regulating cell proliferation or maintaining cells in the postmitotic state.

Our study shows that development of the gcl of the olfactory bulb is delayed in P1 p27KO mice. We also found that the density of apoptotic cells is significantly increased in the gcl of p27KO mice compared with WT mice. This suggests that apoptosis regulates cell survival and contributes to the delayed development of the gcl. In this study, we did not find that SVZa exhibits higher apoptosis compared with other regions, although this region displays the highest proliferation rate. Therefore, in agreement with previous studies (Moreno-Lopez et al., 2004; Lemasson et al., 2005), apoptosis was not affected when SVZ cell proliferation rate was enhanced.

Consistent with a previous report demonstrating that a loss of p27 in the adult SVZ promotes proliferation of transit amplifying cells (Doetsch et al., 2002), we observed enhanced SVZ cell proliferation in the p27KO mouse, as demonstrated by a higher percentage of Ki67+ cells and a higher rate of neurosphere formation than in WT cells. To establish that p27 is a negative regulator of the cell cycle in NPCs of the SVZ, we used a gain-of-function approach. In agreement with our proposed molecular mechanism underlying enhanced cell proliferation in the p27KO mouse, reintroduction of p27 reduced cell proliferation and self-renewal in p27KO SVZ progenitors. Our study also indicates that, in early postnatal SVZ neural progenitors, cell survival is decreased in p27KO neural progenitors under culture conditions that promote cell proliferation, because the number of Caspase 3(+) cells was signifi-

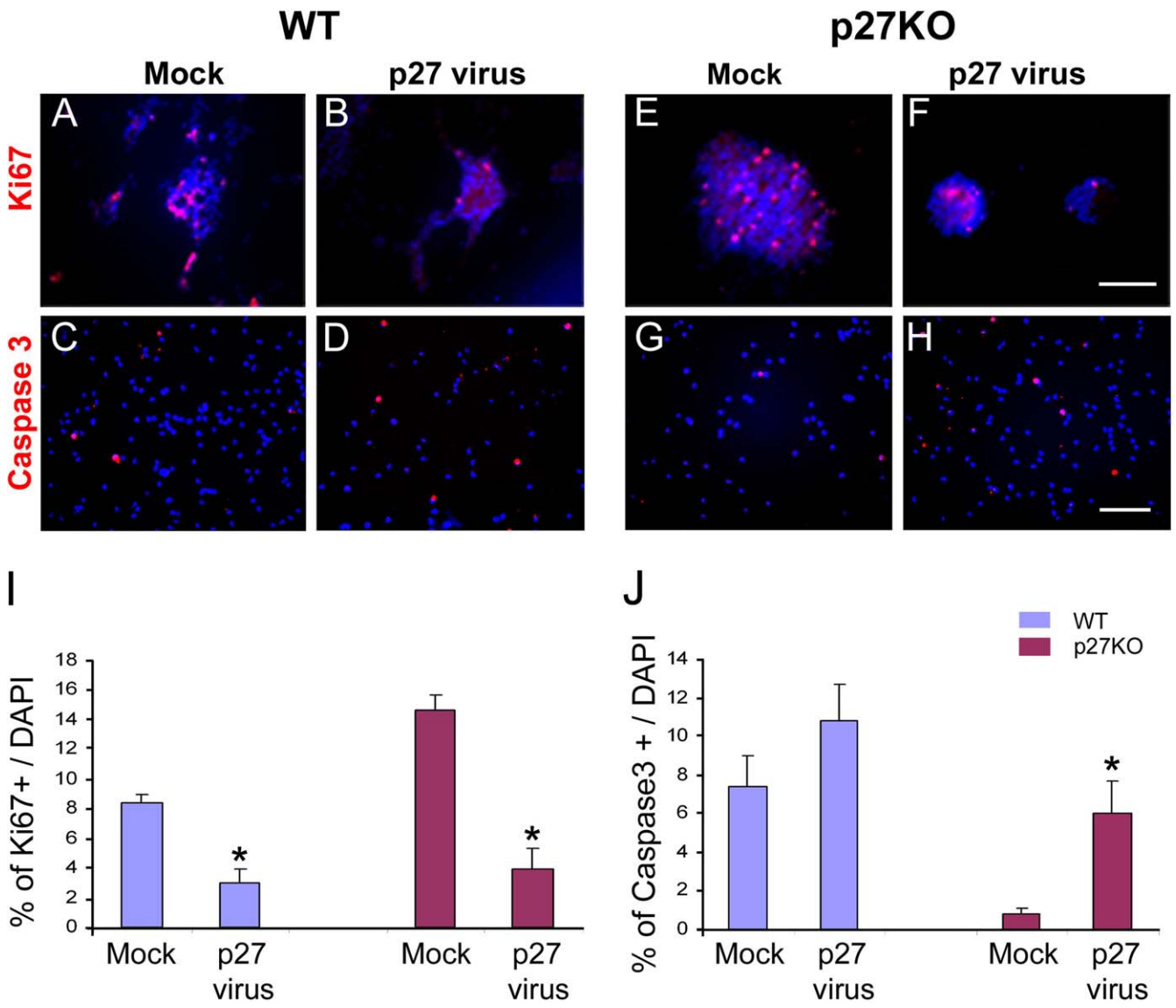

Figure 10. Overexpression of p27 reduces cell proliferation in WT and p27KO NPCs and promotes cell death in p27KO SVZ cells. ***A–H***, SVZ cells from P1 WT and p27KO brains were first cultured and then infected with a mock-retrovirus or a p27-retrovirus. Cells were maintained under culture conditions that promoted cell proliferation for 7 d. Cells were fixed, and imunocytochemistry was performed with anti-Ki67 (***A***, ***B***, ***E***, ***F***) and anti-Caspase 3 (***C***, ***D***, ***G***, ***H***) antibodies. Scale bars: ***A***, ***B***, ***E***, ***F***, 250 μm; ***C***, ***D***, ***G***, ***H***, 100 μm. ***I***, Quantitation of cell proliferation, as determined by anti-Ki67 immunostaining. In both WT and p27KO cells, a reduction in cell proliferation [percentage of Ki67(+) cells] was observed after p27-retrovirus infection compared with mock-retrovirus. ***J***, Quantitation of Caspase 3(+) cells after p27- and mock-retrovirus infection. Note that only in p27KO cells did p27 overexpression increase the percentage of Caspase 3(+) cells. Data were obtained from second and third passage neurospheres of three independent experiments and are expressed as averages + SEM. *$p < 0.03$ (*t* test).

cantly reduced compared with WT cells. This is at variance from previous *in situ* analysis of the adult SVZ (Doetsch et al., 2002); however, this discrepancy could be explained by our parallel finding that in the early postnatal SVZ of the p27KO mouse p21 is upregulated in NPCs. It has been demonstrated that p21 plays an important role in maintaining self-renewal and survival of neural progenitors (Herzog et al., 2002; Kippin et al., 2005; Shi et al., 2005). Additionally, in agreement with Doetsch et al. (2002), we also observed a significant increase in cell death of Tuj1(+) neuroblasts in the RMS and gcl of the olfactory bulb, indicating that p27 is involved in cell survival of committed neuronal progenitors.

CDKs regulate cell proliferation via activation of different molecular targets, including Rb, p107, and p130 (Yoshikawa, 2000). Based on Western blot analysis of SVZ proteins in WT and p27KO mice, we are proposing that CDK2 and Rb play a major role in regulating NPC proliferation in the p27KO mouse SVZ. It is established that Rb activation occurs through hyperphosphorylation of specific amino acid residues, resulting in the release of E2F transcription factors, which play a crucial role in promoting G_1–S transition (Mittnacht, 1998; White et al., 2005; Knudsen and Knudsen, 2006). Indeed, we found that, together with enhanced expression levels of CDK2 and Rb, Rb phosphorylation was also increased in the SVZ of the p27KO mouse, indicating that the CDK2–Rb pathway is engaged in maintaining proliferation of SVZ progenitor cells. Together with an increase in cell proliferation, we also observed lower levels of p21 in the SVZ of p27KO mice, suggesting a reduction in cell differentiation. These data are consistent with studies in which p21, among other CDKIs, was shown to be involved in glial cell differentiation (Durand et al., 1998; Zezula et al., 2001).

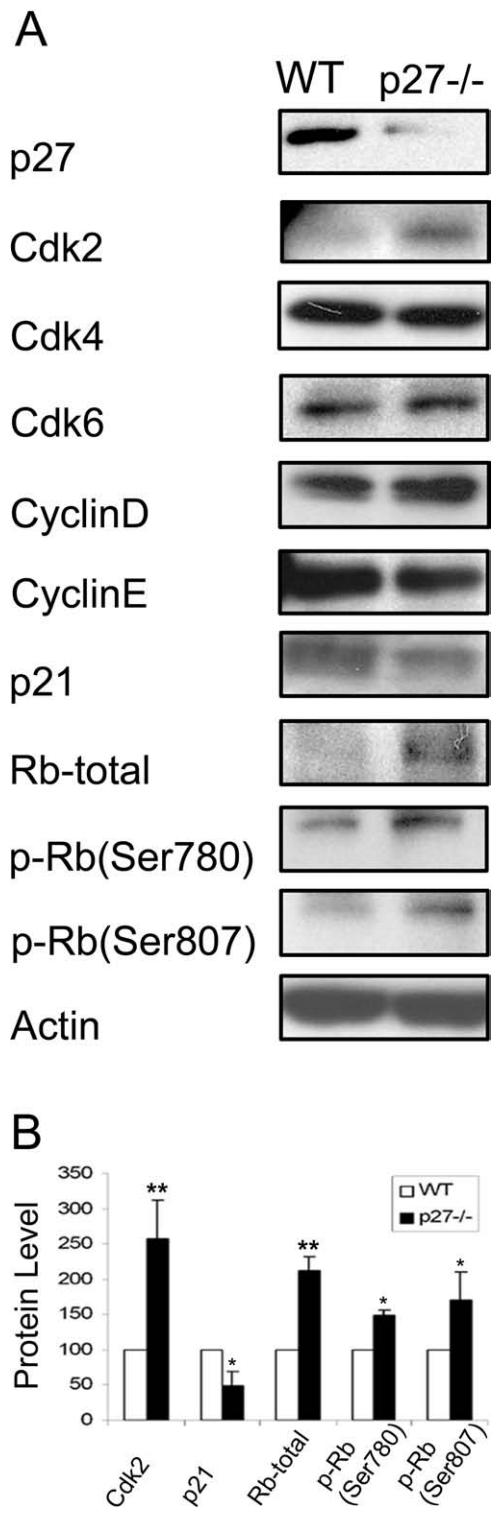

Figure 11. Expression of cell-cycle-related proteins is modified in the p27KO SVZ. Western blot analysis of cell-cycle proteins in SVZ tissue extracts from WT and p27KO mice are shown. ***A***, SVZ tissue was dissected out from P1 WT and p27KO brains. Western blot analysis shows that the phosphorylated forms of Rb [i.e., p-Rb (Ser780) and p-Rb (Ser807)] were elevated in p27KO SVZ compared with WT. CDK2 and total Rb proteins were also increased, whereas p21 was decreased. All lanes were loaded with the same amount of SVZ protein extracts, as shown by actin controls. ***B***, Histograms show normalized protein quantifications for CDK2, p21, total Rb protein, p-Rb (Ser780), and p-Rb (Ser807). CDK4, cyclin D, and cyclin E displayed no significant changes. Data are expressed as means ± SEM obtained from three independent Western blot analyses. $^{**}p < 0.01$; $^{*}p < 0.05$ (*t* test).

In summary, by analyzing early postnatal development of the p27KO mouse, we demonstrate that this CDKI plays a crucial role in regulating cell proliferation and survival in major neurogenic regions of the postnatal brain, including the SVZa, RMS, and olfactory bulb. Our results point to p27 as one of the crucial regulators of postnatal neurogenesis and a putative target for strategies aimed at enhancing neuronal cell repair and regeneration that include either manipulation of endogenous progenitors or transplantation of exogenous undifferentiated neural cells.

References

Aguirre A, Gallo V (2004) Postnatal neurogenesis and gliogenesis in the olfactory bulb from NG2-expressing progenitors of the subventricular zone. J Neurosci 24:10530–10541.

Assoian RK (2004) Stopping and going with p27kip1. Dev Cell 6:458–459.

Bauer S, Rasika S, Han J, Mauduit C, Raccurt M, Morel G, Jourdan F, Benahmed M, Moyse E, Patterson PH (2003) Leukemia inhibitory factor is a key signal for injury-induced neurogenesis in the adult mouse olfactory epithelium. J Neurosci 23:1792–1803.

Besson A, Gurian-West M, Schmidt A, Hall A, Roberts JM (2004) p27Kip1 modulates cell migration through the regulation of RhoA activation. Genes Dev 18:862–876.

Besson A, Gurian-West M, chen X, Kelly-Spratt KS, Kemp CJ, Roberts JM (2006) A pathway in quiescent cells that controls p27Kip1 stability, subcellular localization, and tumor suppression. Genes Dev 20:47–64.

Boehm M, Yoshimoto T, Crook MF, Nallamshetty S, True A, Nabel GJ, Nabel EG (2002) A growth factor-dependent nuclear kinase phosphorylates p27(Kip1) and regulates cell cycle progression. EMBO J 21:3390–3401.

Coskun V, Luskin MB (2001) The expression pattern of the cell cycle inhibitor p19(INK4d) by progenitor cells of the rat embryonic telencephalon and neonatal anterior subventricular zone. J Neurosci 21:3092–3103.

Coskun V, Luskin MB (2002) Intrinsic and extrinsic regulation of the proliferation and differentiation of cells in the rodent rostral migratory stream. J Neurosci Res 69:795–802.

Crean JK, Furlong F, Mitchell D, McArdle E, Godson C, Martin F (2006) Connective tissue growth factor/CCN2 stimulates actin disassembly through Akt/protein kinase B-mediated phosphorylation and cytoplasmic translocation of p27(Kip1). FASEB J 20:1712–1714.

Cunningham JJ, Roussel MF (2001) Cyclin-dependent kinase inhibitors in the development of the central nervous system. Cell Growth Differ 12:387–396.

Cunningham JJ, Levine EM, Zindy F, Goloubeva O, Roussel MF, Smeyne RJ (2002) The cyclin-dependent kinase inhibitors p19(Ink4d) and p27(Kip1) are coexpressed in select retinal cells and act cooperatively to control cell cycle exit. Mol Cell Neurosci 19:359–374.

Doetsch F, Verdugo JM, Caille I, Alvarez-Buylla A, Chao MV, Casaccia-Bonnefil P (2002) Lack of the cell-cycle inhibitor p27Kip1 results in selective increase of transit-amplifying cells for adult neurogenesis. J Neurosci 22:2255–2264.

Durand B, Gao FB, Raff M (1997) Accumulation of the cyclin-dependent kinase inhibitor p27/Kip1 and the timing of oligodendrocyte differentiation. EMBO J 16:306–317.

Durand B, Fero ML, Roberts JM, Raff MC (1998) p27Kip1 alters the response of cells to mitogen and is part of a cell-intrinsic timer that arrests the cell cycle and initiates differentiation. Curr Biol 8:431–440.

Dyer MA, Cepko CL (2001) p27Kip1 and p57Kip2 regulate proliferation in distinct retinal progenitor cell populations. J Neurosci 21:4259–4271.

Falls DL, Luskin MB (2006) Neuronal progenitor cells of the mammalian neonatal anterior subventricular zone. In: Neural development and stem cells, Ed 2 (Rao MS, ed), pp 123–142. New York: Humana.

Fero ML, Rivkin M, Tasch M, Porter P, Carow CE, Firpo E, Polyak K, Tsai LH, Broudy V, Perlmutter RM, Kaushansky K, Roberts JM (1996) A syndrome of multiorgan hyperplasia with features of gigantism, tumorigenesis, and female sterility in p27(Kip1)-deficient mice. Cell 85:733–744.

Goto T, Mitsuhashi T, Takahashi T (2004) Altered patterns of neuron production in the p27 knockout mouse. Dev Neurosci 26:208–217.

Hack MA, Saghatelyan A, de Chevigny A, Pfeifer A, Ashery-Padan R, Lledo PM, Gotz M (2005) Neuronal fate determinants of adult olfactory bulb neurogenesis. Nat Neurosci 8:865–872.

Herzog KH, Braun JS, Han SH, Morgan JI (2002) Differential post-

transcriptional regulation of p21WAF1/Cip1 levels in the developing nervous system following gamma-irradiation. Eur J Neurosci 15:627–636.
Hinds JW (1968) Autoradiographic study of histogenesis in the mouse olfactory bulb. I. Time of origin of neurons and neuroglia. J Comp Neurol 134:287–304.
Jablonska B, Aguirre A, Vandenbosch R, Belachew S, Berthet C, Kaldis P, Gallo V (2007) Cdk2 is critical for proliferation and self-renewal of neural progenitor cells in the adult subventricular zone. J Cell Biol, 179:1231–1245.
Kawauchi T, Chihama K, Nabeshima Y, Hoshino M (2006) Cdk5 phosphorylates and stabilizes p27kip1 contributing to actin organization and cortical neuronal migration. Nat Cell Biol 8:17–26.
Kippin TE, Martens DJ, van der Kooy D (2005) p21 loss compromises the relative quiescence of forebrain stem cell proliferation leading to exhaustion of their proliferation capacity. Genes Dev 19:756–767.
Kiyokawa H, Kineman RD, Manova-Todorova KO, Soares VC, Hoffman ES, Ono M, Khanam D, Hayday AC, Frohman LA, Koff A (1996) Enhanced growth of mice lacking the cyclin-dependent kinase inhibitor function of p27(Kip1). Cell 85:721–732.
Knudsen ES, Knudsen KE (2006) Retinoblastoma tumor suppressor: where cancer meets the cell cycle. Exp Biol Med 231:1271–1281.
Kohwi M, Osumi N, Rubenstein JL, Alvarez-Buylla A (2005) Pax6 is required for making specific subpopulations of granule and periglomerular neurons in the olfactory bulb. J Neurosci 25:6997–7003.
Law AK, Pencea V, Buck CR, Luskin MB (1999) Neurogenesis and neuronal migration in the neonatal rat forebrain anterior subventricular zone do not require GFAP-positive astrocytes. Dev Biol 216:622–634.
Legrier ME, Ducray A, Propper A, Chao M, Kastner A (2001) Cell cycle regulation during mouse olfactory neurogenesis. Cell Growth Differ 12:591–601.
Lemasson M, Saghatelyan A, Olivo-Marin JC, Lledo PM (2005) Neonatal and adult neurogenesis provide two distinct populations of newborn neurons to the mouse olfactory bulb. J Neurosci 25:6816–6825.
Levine EM, Close J, Fero M, Ostrovsky A, Reh TA (2000) p27(Kip1) regulates cell cycle withdrawal of late multipotent progenitor cells in the mammalian retina. Dev Biol 219:299–314.
Lois C, Alvarez-Buylla A (1994) Long-distance neuronal migration in the adult mammalian brain. Science 264:1145–1148.
Luskin MB (1993) Restricted proliferation and migration of postnatally generated neurons derived from the forebrain subventricular zone. Neuron 11:173–189.
McAllister SS, Becker-Hapak M, Pintucci G, Pagano M, Dowdy SF (2003) Novel p27(kip1) C-terminal scatter domain mediates Rac-dependent cell migration independent of cell cycle arrest functions. Mol Cell Biol 23:216–228.
Menezes JR, Luskin MB (1994) Expression of neuron-specific tubulin defines a novel population in the proliferative layers of the developing telencephalon. J Neurosci 14:5399–5416.
Menezes JR, Smith CM, Nelson KC, Luskin MB (1995) The division of neuronal progenitor cells during migration in the neonatal mammalian forebrain. Mol Cell Neurosci 6:496–508.
Mittnacht S (1998) Control of pRB phosphorylation. Curr Opin Genet Dev 8:21–27.
Miyazawa K, Himi T, Garcia V, Yamagishi H, Sato S, Ishizaki Y (2000) A role for p27/Kip1 in the control of cerebellar granule cell precursor proliferation. J Neurosci 20:5756–5763.
Molofsky AV, Slutsky SG, Joseph NM, He S, Pardal R, Krishnamurthy J, Sharpless NE, Morrison SJ (2006) Increasing p16INK4a expression decreases forebrain progenitors and neurogenesis during ageing. Nature 443:448–452.
Moreno-Lopez B, Romero-Grimaldi C, Noval JA, Murillo-Carretero M, Matarredona ER, Estrada C (2004) Nitric oxide is a physiological inhibitor of neurogenesis in the adult mouse subventricular zone and olfactory bulb. J Neurosci 24:85–95.
Ng KL, Li JD, Cheng MY, Leslie FM, Lee AG, Zhou QY (2005) Dependence of olfactory bulb neurogenesis on prokineticin 2 signaling. Science 308:1923–1927.
Nguyen L, Besson A, Heng JI, Schuurmans C, Teboul L, Parras C, Philpott A, Roberts JM, Guillemot F (2006) p27kip1 independently promotes neuronal differentiation and migration in the cerebral cortex. Genes Dev 20:1511–1524.
Nguyen-Ba-Charvet KT, Picard-Riera N, Tessier-Lavigne M, Baron-Van Evercooren A, Sotelo C, Chedotal A (2004) Multiple roles for slits in the control of cell migration in the rostral migratory stream. J Neurosci 24:1497–1506.
Orend G, Hunter T, Ruoslahti E (1998) Cytoplasmic displacement of cyclin E-cdk2 inhibitors p21Cip1 and p27Kip1 in anchorage-independent cells. Oncogene 16:2575–2583.
Padmanabhan J, Park DS, Greene LA, Shelanski ML (1999) Role of cell cycle regulatory proteins in cerebellar granule neuron apoptosis. J Neurosci 19:8747–8756.
Reiner O, Sapir T (2006) Cdk5 checks p27kip1 in neuronal migration. Nat Cell Biol 8:11–13.
Reynisdottir I, Massague J (1997) The subcellular locations of p15(Ink4b) and p27(Kip1) coordinate their inhibitory interactions with cdk4 and cdk2. Genes Dev 11:492–503.
Reynolds BA, Weiss S (1992) Generation of neurons and astrocytes from isolated cells of the adult mammalian central nervous system. Science 255:1707–1710.
Rochefort C, Cheusiu G, Vincent JD, Lledo PM (2002) Enriched odor exposure increases the number of newborn neurons in the adult olfactory bulb and improves odor memory. J Neurosci 22:2679–2689.
Rodier G, Montagnoli A, Di Marcotullio L, Coulombe P, Draetta GF, Pagano M, Meloche S (2001) p27 cytoplasmic localization is regulated by phosphorylation on Ser10 and is not a prerequisite for its proteolysis. EMBO J 20:6672–6682.
Saghatelyan A, de Chevigny A, Schachner M, Lledo PM (2004) Tenascin-R mediates activity-dependent recruitment of neuroblasts in the adult mouse forebrain. Nat Neurosci 7:347–356.
Sherr CJ, Roberts JM (1995) Inhibitors of mammalian G1 cyclin-dependent kinases. Genes Dev 9:1149–1163.
Shi L, Zhao G, Qiu D, Godfrey WR, Vogel H, Rando TA, Hu H, Kao PN (2005) NF90 regulates cell cycle exit and terminal myogenic differentiation by direct binding to the 3′-untranslated region of MyoD and p21WAF1/CIP1 mRNAs. J Biol Chem 280:18981–18989.
Siegenthaler JA, Miller MW (2005) Transforming growth factor β 1 promotes cell cycle exit through the cyclin-dependent kinase inhibitor p21 in the developing cerebral cortex. J Neurosci 25:8627–8636.
Smith CM, Luskin MB (1998) Cell cycle length of olfactory bulb neuronal progenitors in the rostral migratory stream. Dev Dyn 213:220–227.
Tang X, Falls DL, Li X, Lane T, Luskin MB (2007) Antigen-retrieval procedure for bromodeoxyuridine immunolabeling with concurrent labeling of nuclear DNA and antigens damaged by HCl pretreatment. J Neurosci 27:5837–5844.
Temple S, Alvarez-Buylla A (1999) Stem cells in the adult mammalian central nervous system. Curr Opin Neuroiol 9:135–141.
Tomoda K, Kubota Y, Kato J (1999) Degradation of the cyclin-dependent-kinase inhibitor p27Kip1 is instigated by Jab1. Nature 398:160–165.
van Lookeren Campagne M, Gill R (1998) Tumor-suppressor p53 is expressed in proliferating and newly formed neurons of the embryonic and postnatal rat brain: comparison with expression of the cell cycle regulators p21Waf1/Cip1, p27Kip1, p57Kip2, p16Ink4a, cyclin G1, and the proto-oncogene Bax. J Comp Neurol 397:181–198.
White J, Stead E, Faast R, Conn S, Cartwright P, Dalton S (2005) Developmental activation of the Rb-E2F pathway and establishment of cell cycle-regulated cyclin-dependent kinase activity during embryonic stem cell differentiation. Mol Biol Cell 16:2018–20127.
Wu FY, Wang SE, Sanders ME, Shin I, Rojo F, Baselga J, Arteaga CL (2006) Reduction of cytosolic p27(Kip1) inhibits cancer cell motility, survival, and tumorigenicity. Cancer Res 66:2162–2172.
Yoshikawa K (2000) Cell cycle regulators in neural stem cells and postmitotic neurons. Neurosci Res 37:1–14.
Zezula J, Casaccia-Bonnefil P, Ezhevsky SA, Osterhout DJ, Levine JM, Dowdy SF, Chao MV, Koff A (2001) p21cip1 is required for the differentiation of oligodendrocytes independently of cell cycle withdrawal. EMBO Rep 2:27–34.
Zindy F, Cunningham JJ, Sherr CJ, Jogal S, Smeyne RJ, Roussel MF (1999) Postnatal neuronal proliferation in mice lacking Ink4d and Kip1 inhibitors of cyclin-dependent kinases. Proc Natl Acad Sci U S A 96:13462–13467.